

Emerging chiral edge states from the confinement of a magnetic Weyl semimetal in $\text{Co}_3\text{Sn}_2\text{S}_2$

Lukas Muechler,¹ Enke Liu,^{2,3} Jacob Gayles,² Qiunan Xu,² Claudia Felser,^{2,*} and Yan Sun^{2,†}

¹*Center for Computational Quantum Physics, The Flatiron Institute, New York, New York, 10010, USA*

²*Max Planck Institute for Chemical Physics of Solids, D-01187 Dresden, Germany*

³*Institute of Physics, Chinese Academy of Sciences, Beijing 100190, China*

(Dated: March 26, 2020)

The quantum anomalous Hall effect (QAHE) and magnetic Weyl semimetals (WSMs) are topological states induced by intrinsic magnetic moments and spin-orbit coupling. Their similarity suggests the possibility of achieving the QAHE by dimensional confinement of a magnetic WSM along one direction. In this study, we investigate the emergence of the QAHE in the two-dimensional (2D) limit of magnetic WSMs due to finite size effects in thin films and step-edges. We demonstrate the feasibility of this approach with effective models and real materials. To this end, we have chosen the layered magnetic WSM $\text{Co}_3\text{Sn}_2\text{S}_2$, which features a large anomalous Hall conductivity and anomalous Hall angle in its 3D bulk, as our material candidate. In the 2D limit of $\text{Co}_3\text{Sn}_2\text{S}_2$ two QAHE states exist depending on the stoichiometry of the 2D layer. One is a semimetal with a Chern number of 6, and the other is an insulator with a Chern number of 3. The latter has a band gap of 0.05 eV, which is much larger than that in magnetically doped topological insulators. Our findings naturally explain the existence of chiral states in step edges of bulk $\text{Co}_3\text{Sn}_2\text{S}_2$ which have been reported in a recent experiment at $T = 4\text{K}$ and present a realistic avenue to realize QAH states in thin films of magnetic WSMs.

I. INTRODUCTION

The quantum anomalous Hall effect (QAHE) is the quantized version of the anomalous Hall effect (AHE). In the QAHE, the transverse anomalous Hall conductance (AHC) is quantized in units of e^2/h and the longitudinal resistance is reduced to zero¹⁻⁴. In contrast to the ordinary AHE, the QAHE is topologically protected, and is characterized by a non-zero Chern number n and chiral edge states in the bulk band gap. Contrary to the quantum Hall effect, which features the formation of Landau levels induced by an external magnetic field, the QAHE originates from intrinsic magnetic moments and spin orbit coupling (SOC). Because of the absence of back scattering, the electron currents carried by the edge states cannot be dissipated⁵. Therefore, realization of the QAHE and the utilization of its chiral edge state may lead to new low energy consumption quantum electronic devices. It was further proposed that interfaces of QAHE states and superconductors can generate chiral Majorana Fermions (MFs)⁶ via the proximity effect. These MFs are thought to be a fundamental ingredient for the development of topological quantum computing.

The QAHE was first proposed in 1988 by F. D. M. Haldane via a theoretical model defined on a honeycomb lattice⁴. However, because of the special requirements of this model, the realization of the QAHE in real materials took more than twenty years to achieve. Thanks to developments in topological band theory and thin film growth techniques, the effect was observed in counterparts of the QAHE, the quantum spin Hall effect (QSHE) and topological insulators (TIs). The first QAHE was observed in chromium-doped $(\text{Bi,Sb})_2\text{Te}_3$, where the TI gains magnetic order through Van Vleck paramagnetism^{7,8}. Based on the chiral edge states orig-

inating from Cr-doped $(\text{Bi,Sb})_2\text{Te}_3$, chiral MFs were recently observed in the heterostructure of QAHE states and superconductors, which created strong enthusiasm for the comprehensive study of the QAHE and MFs using both theoretical and experimental approaches⁹⁻¹³.

Besides magnetically doped topological insulators^{7,8,14}, much effort was also devoted to the search for new QAHE materials based on different mechanisms¹⁰⁻¹³, such as magnetic and antiferromagnetic semiconductors¹⁵⁻¹⁷, heterostructures of topological insulators (TIs) and ferromagnetic insulators¹⁸⁻²³, heterostructures of heavy atom layers and magnets²⁴⁻²⁸, honeycomb lattice (like graphene, silicene, and transition metal oxide with perovskite structure and pyrochlore oxide along (111) direction) with proximity coupling to ferromagnetic and antiferromagnetic insulators²⁹⁻⁴², as well as thin films of 3D magnetic topological states⁴³, and absorption of atoms on quantum spin Hall insulators⁴⁴, etc. For example, a gap around 100 meV was observed by ARPES in the heterostructure of $\text{MnBi}_2\text{Se}_4/\text{Bi}_2\text{Se}_3$ ⁴⁵.

Recently, another topological metallic state, the Weyl semimetal (WSM), was experimentally determined^{46,47}. Magnetic WSM with layered structures can be understood as coupled 2D QAHE layers^{48,49}. Motivated by this understanding and the development of WSMs, we propose another method of efficiently realizing the QAHE state in a real material. In WSMs, the conduction and valence bands linearly touch each other in 3D momentum space at Weyl points, which behave as monopoles of Berry curvatures with positive and negative chirality. According to symmetries, WSMs can be classified into two groups, those with and without time reversal symmetry. Since the Berry curvature is odd under time reversal, the magnetic WSMs often host a strong AHE originating from the Weyl points. Since

Weyl points can only be defined in 3D momentum space, they require translation symmetry in 3D. Therefore, the Weyl point can be removed by opening a band gap through the breaking of periodic boundary conditions along one direction. If band ordering is maintained during this procedure, it is possible to obtain a QAHE phase in the 2D limit of the magnetic WSMs. On the other hand, since the QAHE exists only in the extreme 2D limit, magnetic WSMs with layered crystal structures are preferred material candidates.

II. OUTLINE

The paper is organized as follows: In Sec. III we review the proposal to realize a QAH state in thin films of a magnetic WSM based on model calculations. Using ab-initio calculations, we show in Sec. IV that thin films of the magnetic WSM $\text{Co}_3\text{Sn}_2\text{S}_2$ are ideal candidates to realize the QAH state in two different stoichiometries. In the last section (Sec. V), we discuss how these findings explain the recent observation of chiral modes on step edges of bulk $\text{Co}_3\text{Sn}_2\text{S}_2$.

III. MODEL DISCUSSION

To evaluate the feasibility of this proposal, we first analyzed the 2D limit of the Weyl semimetal using a toy two band model, $H = A(k_x\sigma(x) + k_y\sigma(y)) + M(k)\sigma_z$, with $M(k) = M_0 - M_1(k_x^2 + k_y^2 + k_z^2)^{50}$. As shown in Fig. 1(a), this model describes a magnetic WSM with one pair of Weyl points located at $\pm k_W$ along the k_z -axis and the Fermi level (E_F) lies just at the Weyl point. Owing to the Berry flux between this pair of Weyl points, the anomalous Hall conductivity reaches a peak value at E_F with $\sigma_{AH} = (k_w/\pi)(e^2/h)$, which is proportional to the separation of the Weyl points, see Fig. 1 (b) and (c)⁵⁰. Breaking the periodic boundary condition in the z direction, the Weyl points are removed by the opening of the band gap. Depending on the interaction strength between the top and bottom sides of the film, the band order can change as the thickness varies, resulting in a quantized jump of the AHC from zero to a finite number. From the parameters specified in this study, the interactions between the top and bottom surfaces remove the band inversion of the 3D bulk state for thicknesses of one and two unit cells. Upon increasing the film thickness above three unit cells, the quantum confinement effect weakens and the band inversion remains, which leads to a quantized AHC and chiral edge state in the band gap, as shown in Fig. 1(df). Therefore, the mechanism for obtaining the QAHE from magnetic WSMs is principally allowed, but its realization from available materials remains challenging.

To date, many theoretical magnetic WSMs have been proposed, some of which feature strong AHEs^{48,51-54}.

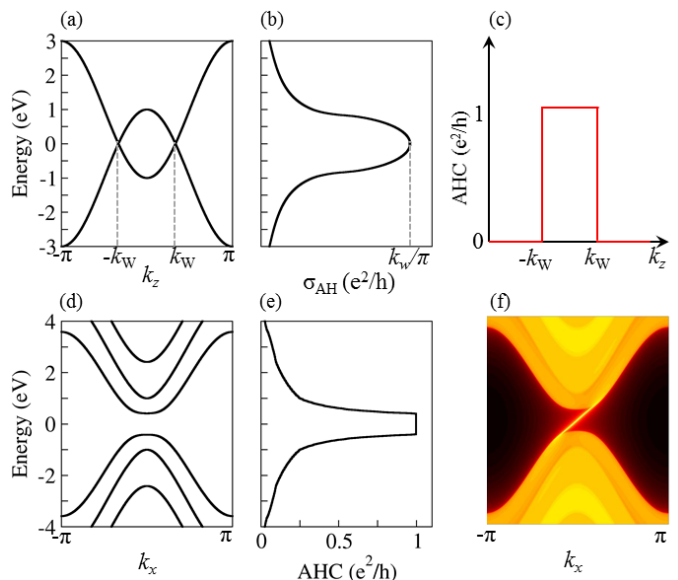


FIG. 1. (a) Energy dispersion along k_z and (b) energy dependent anomalous Hall conductivity in the WSM effective model. (c) A quantized 2D-anomalous Hall conductance (AHC) exists between a pair of Weyl points for fixed k_z between $-k_w < k_z < k_w$. (d) Energy dispersion of the film from the WSM effective model with a thickness of three unit cells. (e) The anomalous Hall conductivity (AHC) is quantized in the band gap of the film. (f) Energy dispersion of the edge states of the film. We have projected the $k \cdot p$ model to a cubic lattice with a lattice constant of 1 \AA , and parameters of $A=1.0 \text{ eV \AA}$, $M_0=1 \text{ eV}$, and $M_1=1 \text{ eV \AA}^2$

Since the QAHE is a 2D insulator, WSMs with large AHE, low charge carrier density, and layered lattice structure are preferred. In this study, we choose the experimentally well characterized quasi-2D material $\text{Co}_3\text{Sn}_2\text{S}_2$ to examine the possibility of realizing a QAHE based on a magnetic WSM. $\text{Co}_3\text{Sn}_2\text{S}_2$ is a half metal with a rhombohedral lattice structure in the space group $R\bar{3}m$ (No. 166)⁵⁵⁻⁵⁷. The magnetic Co atoms are arranged in a Kagome lattice in the $x - y$ plane with magnetic moments along the z axis. When the lattice is placed in a hexagonal setting, Co_3Sn forms a quasi-2D layer and a sandwich between the S atoms. The quasi-2D layer Co_3Sn_2 are connected by another Sn atom in the z direction, as shown in Fig. 2(a).

IV. SINGLE LAYER LIMIT

Recently, large anomalous Hall conductivities up to 1100 S/cm were observed in $\text{Co}_3\text{Sn}_2\text{S}_2$, originating from the SOC induced node-line-like band anticrossings and Weyl points, see Fig. 2(c, d). Owing to the low charge carrier density, the anomalous Hall angle reaches as high as 20%, which has not been observed in other compounds^{58,59}. In this material, the Weyl points are very close to E_F and there is almost no interference from triv-

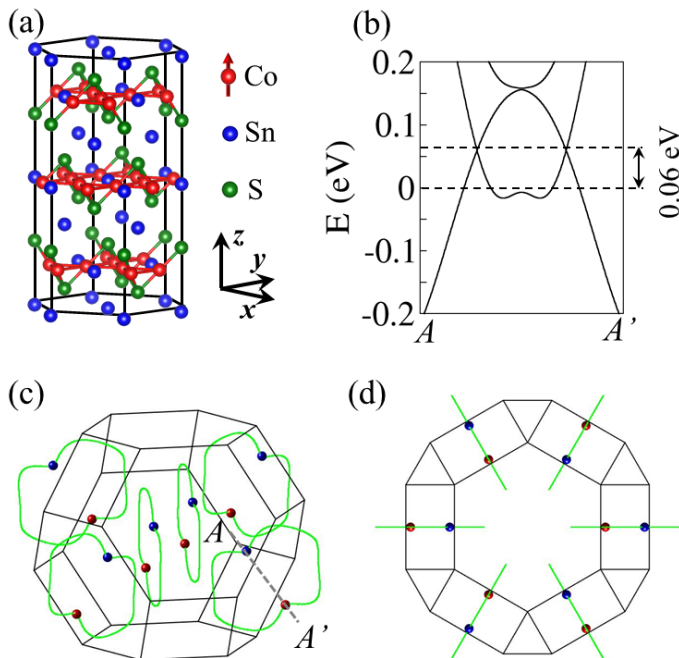


FIG. 2. (a) Lattice structure of $\text{Co}_3\text{Sn}_2\text{S}_2$. The spin polarization of the Co atom is along the z direction. (b) Energy dispersion of $\text{Co}_3\text{Sn}_2\text{S}_2$ along one pair of Weyl points with opposite chirality. The labels for the k points are given in (c). (c, d) Side view and top view of the nodal lines and Weyl points distribution in BZ, respectively. The red and blue dots represent opposite chirality of the Weyl points.

ial bands, in contrast to other proposed magnetic WSMs. These properties make $\text{Co}_3\text{Sn}_2\text{S}_2$ an ideal candidate to realize a QAH state with chiral edge modes in the 2D limit due to finite size effects. Because of the weak bonding between Sn and $\text{Co}_3\text{Sn}_2\text{S}_2$ layers, it should be possible to achieve the 2D films and step states by breaking the weak bonds. Therefore, $\text{Co}_3\text{Sn}_2\text{S}_2$ provides an ideal platform to study the interplay between the QAHE and WSMs experimentally.

Two possible terminations exist for cleaved $\text{Co}_3\text{Sn}_2\text{S}_2$, one with a Sn termination and the other with a S termination. The Co atoms form a Kagome lattice, with the Sn atom in the center. Sandwiching the Kagome lattice of Co_3Sn between two S layers, a minimized thickness can be obtained for the S-terminated $\text{Co}_3\text{Sn}_2\text{S}_2$ film, see Fig. 3(a). By further sandwiching the $\text{Co}_3\text{Sn}_2\text{S}_2$ with neighboring Sn layers, the other minimum thickness can be obtained for the Sn-terminated $\text{Co}_3\text{Sn}_3\text{S}_2$ film. To obtain the magnetic ground state, the total energies of magnetization along the (001), (100), (010), and (110) directions were compared for both the bulk state and the two possible structures for the monolayers via density functional theory (DFT) calculations^{60,61}. For the bulk state, the total energy in (001) phase is around 1.4 meV lower than that with magnetization oriented in the $x-y$ plane, which is consistent with the experimental measurements^{56,58,59}. Similarly, the two monolayer struc-

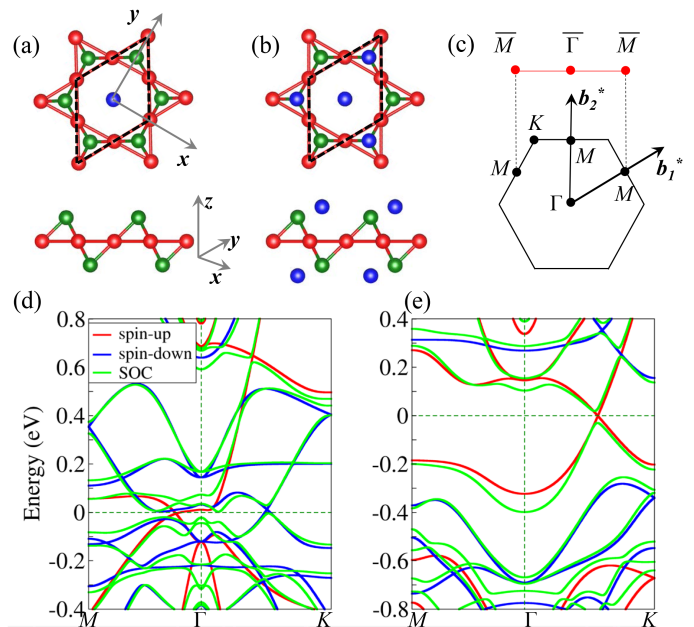


FIG. 3. Lattice structure of (a) $\text{Co}_3\text{Sn}_2\text{S}_2$ and (b) $\text{Co}_3\text{Sn}_3\text{S}_2$ films from the top (upper panel) and side (lower panel) view. (c) Corresponding 2D BZ and its 1D projection. The energy dispersion along high symmetry lines as shown for (d) $\text{Co}_3\text{Sn}_2\text{S}_2$ and (e) $\text{Co}_3\text{Sn}_3\text{S}_2$ with and without the inclusion of SOC.

tures also preferred a magnetic structure with magnetization along the (001) direction, however the energy differences are only around 0.4 and 0.1 meV in $\text{Co}_3\text{Sn}_3\text{S}_2$ and $\text{Co}_3\text{Sn}_2\text{S}_2$ films, respectively, much lower than in the bulk with $T_c \simeq 200\text{K}$. Owing to the 2D magnetic structure and the small anisotropic energy, the dipole-dipole interaction might play an important role for the spin oriented in plane. However, the dipole-dipole interaction is around one order of magnitude weaker than the anisotropic energy, due to the small moment of the Co ions. see Fig. 4. Therefore, the magnetic are expected to along (001) direction. Based on the anisotropic energy, the magnetic order temperature for $\text{Co}_3\text{Sn}_3\text{S}_2$ and $\text{Co}_3\text{Sn}_2\text{S}_2$ freestanding monolayers are around 5.0 and 1.0 K, respectively. The anisotropy can increase in the presence of a substrate, which in turn can increase the ordering temperature.

Without SOC, the $\text{Co}_3\text{Sn}_2\text{S}_2$ film shows a semi-metallic band structure. In contrast to the half-metallic state in the 3D bulk, both spin-up and spin-down channels appear close to the Fermi level in the $\text{Co}_3\text{Sn}_2\text{S}_2$ films. Owing to the mirror planes of M_x and M_y , both spin-up and spin-down channels form the linear band crossing around E_F , which exist on the high symmetry lines along $M-\Gamma$ and $\Gamma-K$, respectively, see Fig. 3(d). After SOC is considered, the $\text{SU}(2)$ symmetry is broken, leading to gapping of the linear band crossings.

Viewing the energy dispersion in a larger energy window, it is clear that another linear band exists crossing

TABLE I. The comparison of total energies with magnetic polarization along (001) and other directions. The energy differences are in the unit of of meV/(formula unit).

	$E_{tot}(100)-E_{tot}(001)$	$E_{tot}(010)-E_{tot}(001)$	$E_{tot}(110)-E_{tot}(001)$
$\text{Co}_9\text{Sn}_6\text{S}_6$ (bulk)	1.4	1.4	1.4
$\text{Co}_3\text{Sn}_3\text{S}_2$	0.5	0.4	0.4
Co_3SnS_2	0.2	0.2	0.1

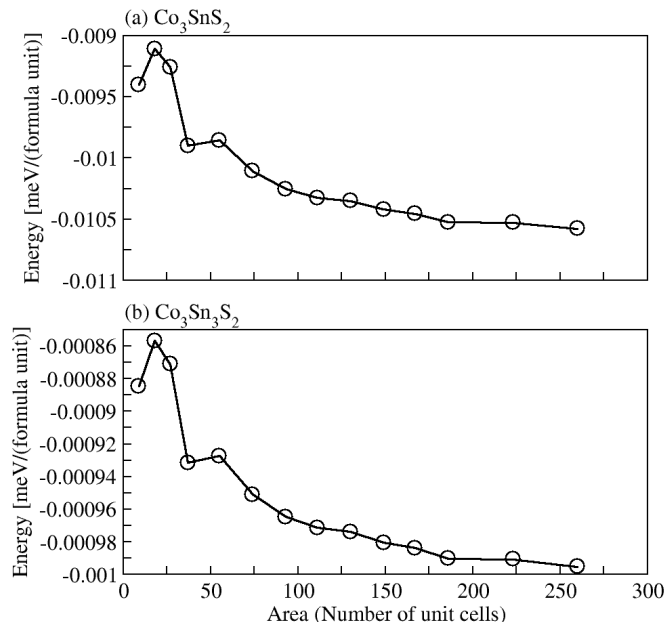


FIG. 4. Convergence of the dipole-dipole interaction along with the increasing of number of in-plane unit cells.

$\Gamma - K$ with its chemical potential shifting up by approximately 0.6 eV and 4 electrons, corresponding to the filling expected for films with Sn termination. This system should act as a semi-metal from the perspective of transport, by simply shifting the chemical potential to the upper linear band crossing point, see Fig. 3(d). However, the Sn layers affect the filling and change the dispersion of the bands around E_F . As shown in Fig. 3 (e), after further sandwiching by Sn layers, the system has an ideal semi-metallic state with the Fermi surface composed solely of the linear crossing points. Similar to Co_3SnS_2 , this linear band crossing is broken by SOC with the opening of a band gap. Compared to Co_3SnS_2 , the Sn terminated film has a global band gap at approximately 0.05 eV, which is much larger than that in magnetic-impurity-doped TIs.

To confirm the quantization of the anomalous Hall conductance (AHC), we calculated the energy dependent AHC by integrating the Berry curvature over the whole BZ. The AHC for Co_3SnS_2 can reach up to almost $6 e^2/h$ at the charge neutral point. However, since Co_3SnS_2 does not have a global band gap, its AHC changes sharply as the energy varies around E_F , and the maximum value only appears at an energy point, see Fig. 5(a). Though

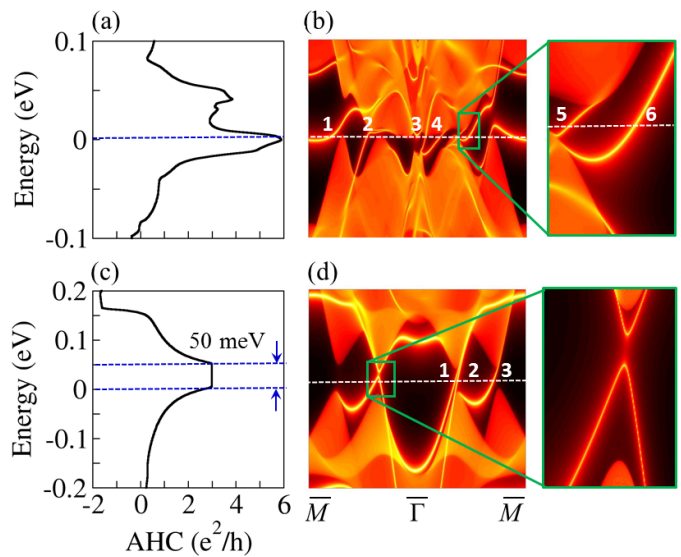


FIG. 5. (a, b) Energy dependent AHC for the Co_3SnS_2 film. The peak value with $\text{AHC}=6 e^2/h$ appears at a charge neutral point. (b) Energy dispersion of the edge states for the Co_3SnS_2 film. The local energy dispersion around edge states No.5 and No.6 are given on the right. (c) Quantized AHC ($3 e^2/h$) appears in the band gap for the $\text{Co}_3\text{Sn}_3\text{S}_2$ film. (d) Edge states of $\text{Co}_3\text{Sn}_3\text{S}_2$ film. The trivial dangling bond states are zoomed in on the right side.

$\text{Co}_3\text{Sn}_3\text{S}_2$ has four more electrons than Co_3SnS_2 , only three of them have non-zero Chern number (-1), leading to the Chern number jump from 6 to 3. In contrast the semimetallic state in Co_3SnS_2 , the film with a stoichiometry of $\text{Co}_3\text{Sn}_3\text{S}_2$ has a constant quantized AHC in the energy range from E_F to E_F+50 meV, as shown in Fig. 5(c). Thus, both the Co_3SnS_2 and $\text{Co}_3\text{Sn}_3\text{S}_2$ films host nontrivial topological electronic structures with non-zero Chern numbers of 6 and 3, respectively.

A typical feature of the quantum anomalous Hall insulators and semi-metals is their chiral edge state. To calculate the edge states, we projected the Bloch wave functions into Wannier orbitals⁶², and constructed a tight binding model Hamiltonian. The edge state was considered under open boundary conditions with the half-infinite one-dimensional model using the iterative Greens function method^{63,64}. The energy dispersions of the edge states for films with the nominal compositions Co_3SnS_2 and $\text{Co}_3\text{Sn}_3\text{S}_2$ are shown in Fig. 5(b) and (d), respectively. Due to the semi-metallic properties of the mono-

layers with the stoichiometry Co_3SnS_2 , the projections of the bulk conduction and valence are separated by a gap, which are connected by six edge bands. The edge bands all possess a positive Fermi velocity, corresponding to a Chern number of 6. In the monolayers with the stoichiometry $\text{Co}_3\text{Sn}_3\text{S}_2$, three topological protected channels exist on the edge with positive Fermi velocity, which is consistent with a Chern number of 3 obtained from the calculation of the quantized AHC, see Fig. 5(d). Since the properties of the edge states are strongly dependent on the nature of the edge termination, the topological edge-states can be distinguished from trivial dangling bond states, since the dangling bonds are not topologically protected. They do not connect the valence and conduction states of the bulk, as can be seen in the zoom in in Fig. 5(d), and should be easily annihilated by chemical engineering of the edge termination.

V. CHIRAL MODES AT STEP EDGES

Although a QAHE is expected in monolayers of the stoichiometry Co_3SnS_2 and $\text{Co}_3\text{Sn}_3\text{S}_2$, their free standing form is not expected to be stable without a substrate, indicated by phonon frequencies of the free standing slabs. A suitable substrate could stabilize these monolayers at higher temperatures due to kinetic effects, however this is beyond the possibilities of DFT to predict and requires additional experimental input. However, our results further imply the presence of chiral modes at step edges on bulk $\text{Co}_3\text{Sn}_2\text{S}_2$, which could be easily measured by STM experiments. A step edge can be modeled as a single QAH layer that is coupled to the bulk WSM. If the coupling between the QAH layer and the bulk can be treated perturbatively as expected in a layered material, the step edge is expected to host chiral edge states, similarly to the QSH step edge states observed in WTe_2 ⁶⁵. Even in the case of stronger coupling between the layers, the 'terrace construction' of Hsieh *et al.*⁶⁶ suggests the presence of spatially separated, counterpropagating chiral states at step edges that could be observed in STM experiments, as the combined Chern number of the top layer and WSM has to vanish. In this setup, one would expect to observe the edge states at temperatures close to the bulk $T_c \simeq 200\text{K}$, which could open a pathway to more

detailed studies of topological chiral states at higher temperatures. Indeed, such states have recently been reported in STM experiments on step-edges at $T = 4\text{K}$ ⁶⁷ as a direct consequence of the topological non-trivial electronic structure in the thin film limit.

VI. SUMMARY

In summary, we theoretically studied the QAHE from the quantum confinement of the magnetic WSMs. Since the WSM can only be defined in 3D momentum space, a method for the phase transition from WSM to QAHE is breaking the translational symmetry along one direction in the WSM. Considering the 2D topological insulating state in the QAHE, the WSMs with strong AHE, low charge density, and layered lattice structure are preferred candidates. Considering these material requirements, we focused on the layered magnetic WSM $\text{Co}_3\text{Sn}_2\text{S}_2$ as a candidate for the realization of QAHE from WSMs. In the 2D limit of $\text{Co}_3\text{Sn}_2\text{S}_2$, we find two possible QAHE states. One is a semi-metal with a Chern number of 6, and the other is an insulator with a Chern number of 3 and band gap of 0.05 eV. Our findings are supported by the recent observation of chiral modes at step edges of bulk $\text{Co}_3\text{Sn}_2\text{S}_2$, which follows from the non-zero Chern numbers in the 2D limit of $\text{Co}_3\text{Sn}_2\text{S}_2$ ⁶⁷.

ACKNOWLEDGMENTS

This work was financially supported by the ERC Advanced Grant No. 291472 'Idea Heusler', ERC Advanced Grant No. 742068-TOPMAT, and Deutsche Forschungsgemeinschaft DFG under SFB 1143. EL acknowledges support from the Alexander von Humboldt foundation of Germany for his Fellowship and from National Natural Science Foundation of China for his Excellent Young Scholarship (No. 51722106). LM would like to thank the MPI CPFS where part of the work was performed, and the authors thank Binghai Yan for helpful discussions. The Flatiron Institute is a division of the Simons Foundation.

* Claudia.Felser@cpfs.mpg.de

† ysun@cpfs.mpg.de

¹ E. H. Hall, *Amer. J. Math.* **2**, 287 (1879).

² E. H. Hall, *The London, Edinburgh, and Dublin Philosophical Magazine and Journal of Science* **12**, 157 (1881).

³ N. Nagaosa, J. Sinova, S. Onoda, A. H. MacDonald, and N. P. Ong, *Rev. Mod. Phys.* **82**, 1539 (2010).

⁴ F. D. M. Haldane, *Phys. Rev. Lett.* **61**, 2015 (1988).

⁵ B. I. Halperin, *Phys. Rev. B* **25**, 2185 (1982).

⁶ X.-L. Qi, T. L. Hughes, and S.-C. Zhang, *Phys. Rev. B* **82**, 184516 (2010).

⁷ R. Yu, W. Zhang, H.-J. Zhang, S.-C. Zhang, X. Dai, and Z. Fang, *Science* **329**, 61 (2010).

⁸ C.-Z. Chang, J. Zhang, X. Feng, J. Shen, Z. Zhang, M. Guo, K. Li, Y. Ou, P. Wei, L.-L. Wang, *et al.*, *Science* **340**, 167 (2013).

⁹ Q. L. He, L. Pan, A. L. Stern, E. C. Burks, X. Che, G. Yin, J. Wang, B. Lian, Q. Zhou, E. S. Choi, *et al.*, *Science* **357**,

- 294 (2017).
- ¹⁰ C.-X. Liu, S.-C. Zhang, and X.-L. Qi, Annual Review of Condensed Matter Physics **7**, 301 (2016).
 - ¹¹ H. Weng, R. Yu, X. Hu, X. Dai, and Z. Fang, Advances in Physics **64**, 227 (2015).
 - ¹² Y. Ren, Z. Qiao, and Q. Niu, Reports on Progress in Physics **79**, 066501 (2016).
 - ¹³ J. Wang, B. Lian, and S.-C. Zhang, Physica Scripta **2015**, 014003 (2015).
 - ¹⁴ C.-X. Liu, X.-L. Qi, X. Dai, Z. Fang, and S.-C. Zhang, Phys. Rev. Lett. **101**, 146802 (2008).
 - ¹⁵ Q.-F. Liang, L.-H. Wu, and X. Hu, New Journal of Physics **15**, 063031 (2013).
 - ¹⁶ J. He, X. Li, P. Lyu, and P. Nachtigall, Nanoscale **9**, 2246 (2017).
 - ¹⁷ X.-L. Sheng and B. K. Nikoli, Phys. Rev. B **95**, 201402(R) (2017).
 - ¹⁸ S. Eremeev, V. Men'Shov, V. Tugushev, P. M. Echenique, and E. V. Chulkov, Phys. Rev. B **88**, 144430 (2013).
 - ¹⁹ S. Eremeev, V. Men, V. Tugushev, E. V. Chulkov, *et al.*, J. Magn. Magn. Mater. **383**, 30 (2015).
 - ²⁰ F. Katmis, V. Lauter, F. S. Nogueira, B. A. Assaf, M. E. Jamer, P. Wei, B. Satpati, J. W. Freeland, I. Eremin, D. Heiman, *et al.*, Nature **533**, 513 (2016).
 - ²¹ M. M. Otrokov, T. V. Menshchikova, M. G. Vergniory, I. P. Rusinov, A. Y. Vyazovskaya, Y. M. Koroteev, G. Bihlmayer, A. Ernst, P. M. Echenique, A. Arnau, *et al.*, 2D Materials **4**, 025082 (2017).
 - ²² M. Otrokov, T. V. Menshchikova, I. Rusinov, M. Vergniory, V. M. Kuznetsov, and E. V. Chulkov, JETP Letters **105**, 297 (2017).
 - ²³ J. A. Hagmann, X. Li, S. Chowdhury, S.-N. Dong, S. Rouvimov, S. J. Pookpanratana, K. M. Yu, T. A. Orlova, T. B. Bolin, C. U. Segre, *et al.*, New Journal of Physics **19**, 085002 (2017).
 - ²⁴ K. F. Garrity and D. Vanderbilt, Phys. Rev. Lett. **110**, 116802 (2013).
 - ²⁵ K. F. Garrity and D. Vanderbilt, Phys. Rev. B **90**, 121103 (2014).
 - ²⁶ J. Liu, S. Y. Park, K. F. Garrity, and D. Vanderbilt, Phys. Rev. Lett. **117**, 257201 (2016).
 - ²⁷ G. Xu, J. Wang, C. Felser, X.-L. Qi, and S.-C. Zhang, Nano Lett. **15**, 2019 (2015).
 - ²⁸ L. Si, O. Janson, G. Li, Z. Zhong, Z. Liao, G. Koster, and K. Held, Phys. Rev. Lett. **119**, 026402 (2017).
 - ²⁹ Z. Qiao, S. A. Yang, W. Feng, W.-K. Tse, J. Ding, Y. Yao, J. Wang, and Q. Niu, Phys. Rev. B **82**, 161414 (2010).
 - ³⁰ R. Nandkishore and L. Levitov, Phys. Rev. B **82**, 115124 (2010).
 - ³¹ W.-K. Tse, Z. Qiao, Y. Yao, A. H. MacDonald, and Q. Niu, Phys. Rev. B **83**, 155447 (2011).
 - ³² F. Zhang, J. Jung, G. A. Fiete, Q. Niu, and A. H. MacDonald, Phys. Rev. Lett. **106**, 156801 (2011).
 - ³³ M. Ezawa, Phys. Rev. Lett. **109**, 055502 (2012).
 - ³⁴ M. Ezawa, Phys. Rev. Lett. **110**, 026603 (2013).
 - ³⁵ J. Zhang, B. Zhao, Y. Yao, and Z. Yang, Scientific reports **5**, 10629 (2015).
 - ³⁶ J. Zhang, B. Zhao, Y. Yao, and Z. Yang, Phys. Rev. B **92**, 165418 (2015).
 - ³⁷ Z. Qiao, W. Ren, H. Chen, L. Bellaiche, Z. Zhang, A. H. MacDonald, and Q. Niu, Phys. Rev. Lett. **112**, 116404 (2014).
 - ³⁸ D. Xiao, W. Zhu, Y. Ran, N. Nagaosa, and S. Okamoto, Nat. Commun. **2**, 596 (2011).
 - ³⁹ A. Rüegg and G. A. Fiete, Phys. Rev. B **84**, 201103 (2011).
 - ⁴⁰ X. Hu, A. Rüegg, and G. A. Fiete, Phys. Rev. B **86**, 235141 (2012).
 - ⁴¹ A. Zyuzin, S. Wu, and A. Burkov, Phys. Rev. B **85**, 165110 (2012).
 - ⁴² Q.-F. Liang, L.-H. Wu, and X. Hu, New Journal of Physics **15**, 063031 (2013).
 - ⁴³ G. Xu, H. Weng, Z. Wang, X. Dai, and Z. Fang, Phys. Rev. Lett. **107**, 186806 (2011).
 - ⁴⁴ S.-C. Wu, G. Shan, and B. Yan, Phys. Rev. Lett. **113**, 256401 (2014).
 - ⁴⁵ T. Hirahara, S. V. Eremeev, T. Shirasawa, Y. Okuyama, T. Kubo, R. Nakanishi, R. Akiyama, A. Takayama, T. Hagiiri, S.-i. Ideta, *et al.*, Nano Lett. **17**, 3493 (2017).
 - ⁴⁶ S.-Y. Xu, I. Belopolski, N. Alidoust, M. Neupane, G. Bian, C. Zhang, R. Sankar, G. Chang, Z. Yuan, C.-C. Lee, *et al.*, Science **349**, 613 (2015).
 - ⁴⁷ B. Lv, H. Weng, B. Fu, X. Wang, H. Miao, J. Ma, P. Richard, X. Huang, L. Zhao, G. Chen, *et al.*, Physical Review X **5**, 031013 (2015).
 - ⁴⁸ X. Wan, A. M. Turner, A. Vishwanath, and S. Y. Savrasov, Phys. Rev. B **83**, 205101 (2011).
 - ⁴⁹ A. Burkov and L. Balents, Phys. Rev. Lett. **107**, 127205 (2011).
 - ⁵⁰ H.-Z. Lu, S.-B. Z. Zhang, and S.-Q. Shen, Phys. Rev. B **92**, 045203 (2015).
 - ⁵¹ G. Xu, H. Weng, Z. Wang, X. Dai, and Z. Fang, Phys. Rev. Lett. **107**, 186806 (2011).
 - ⁵² Z. Wang, M. Vergniory, S. Kushwaha, M. Hirschberger, E. Chulkov, A. Ernst, N. P. Ong, R. J. Cava, and B. A. Bernevig, Phys. Rev. Lett. **117**, 236401 (2016).
 - ⁵³ T.-R. Chang, G. Chang, C.-C. Lee, S.-M. Huang, B. Wang, G. Bian, H. Zheng, D. S. Sanchez, I. Belopolski, N. Alidoust, M. Neupane, A. Bansil, H.-T. Jeng, S.-Y. Xu, H. Lin, and M. Z. Hasan, Nat. Commun. **7**, 1 (2016).
 - ⁵⁴ J. Kübler and C. Felser, EPL (Europhysics Letters) **114**, 47005 (2016).
 - ⁵⁵ R. Wehrich, I. Anusca, and M. Zabel, ChemInform **36**, 35 (2005).
 - ⁵⁶ P. Vaquero and G. G. Sobany, Solid State Sci. **11**, 513 (2009).
 - ⁵⁷ W. Schnelle, A. Leithe-Jasper, H. Rosner, F. Schappacher, R. Pöttgen, F. Pielnhofer, and R. Wehrich, Phys. Rev. B **88**, 144404 (2013).
 - ⁵⁸ E. Liu, Y. Sun, N. Kumar, L. Muechler, A. Sun, L. Jiao, S.-Y. Yang, D. Liu, A. Liang, Q. Xu, *et al.*, Nat. Phys. **14**, 1125 (2018).
 - ⁵⁹ Q. Wang, Y. Xu, R. Lou, Z. Liu, M. Li, Y. Huang, D. Shen, H. Weng, S. Wang, and H. Lei, Nat. Commun. **9**, 3681 (2018).
 - ⁶⁰ G. Kresse and J. Furthmüller, Phys. Rev. B **54**, 11169 (1996).
 - ⁶¹ J. P. Perdew, K. Burke, and M. Ernzerhof, Phys. Rev. Lett. **77**, 3865 (1996).
 - ⁶² A. A. Mostofi, J. R. Yates, Y.-S. Lee, I. Souza, D. Vanderbilt, and N. Marzari, Comput. Phys. Commun. **178**, 685 (2008).
 - ⁶³ M. L. Sancho, J. L. Sancho, and J. Rubio, J. Phys. F Met. Phys. **14**, 1205 (1984).
 - ⁶⁴ M. L. Sancho, J. L. Sancho, J. L. Sancho, and J. Rubio, J. Phys. F Met. Phys. **15**, 851 (1985).
 - ⁶⁵ L. Peng, Y. Yuan, G. Li, X. Yang, J.-J. Xian, C.-J. Yi, Y.-G. Shi, and Y.-S. Fu, Nat. Commun. **8**, 659 (2017).

- ⁶⁶ T. H. Hsieh, H. Ishizuka, L. Balents, and T. L. Hughes, Phys. Rev. Lett. **116**, 086802 (2016). arXiv:1910.11205 (2019).
- ⁶⁷ S. Howard, L. Jiao, Z. Wang, P. Vir, C. Shekhar, C. Felser, T. Hughes, and V. Madhavan, arXiv preprint